www.adeepakpublishing.com

Mayank, et al. (2026): JoSS, Vol. 15, No. 1, pp. 1299–1318
(Peer-reviewed article available at www.jossonline.com)

www. JoSSonline.com

Testing and Validation of Transparent Materials for Solar Cell Integrated Satellite Antenna

Mayank, Ville Lunden, Anton Fetzer, Jari Holopainen, Jaan Praks
Department of Electronics and Nanoengineering, Aalto University
Espoo, Finland

Johannes Schumacher
Celestial Space Technologies GmbH
Nürnberg, Germany

Abstract

The continued miniaturization of spacecraft demands efficient utilization of spacecraft resources, including their limited surface area, over which antennas and solar cells often compete. To address this challenge, various optically transparent antennas have been proposed to enable simultaneous dual use of the spacecraft surface for RF antenna applications and power generation. This current work presents a new solar cell-integrated patch antenna design for C-band at 4.3 GHz. The materials used in this work – a transparent polymethylpentene (PMP) substrate and a conductive hybrid carbon nanotube (CNT) and silver thin film – present improved radio frequency (RF) and optical transmissivity properties compared to materials previously used for such antennas. The prototype antenna uses a space-grade mono-crystalline silicon solar cell selected primarily based on availability, as simulations suggest that the solar cell type does not significantly affect the antenna RF performance, and the optical passband region of the antenna covers the operating wavelength band of both silicon and higher efficiency gallium arsenide (GaAs) solar cells, making these cell types effectively interchangeable considering the results of this work. To preliminarily validate the new antenna design and materials for space conditions, the antenna is subjected to an environmental test campaign consisting of total ionizing dose (TID) gamma-ray irradiation and thermal vacuum (TVAC) cycling. The antenna RF properties and optical transmissivity are measured before and after the environmental tests for validation. Also, the outgassing properties of the antenna are considered by measuring the total mass loss (TLM) of the antenna system caused by TVAC tests. The proposed antenna demonstrates a balance between radiation efficiency (81%) and high optical transmissivity (71.6%), not shown by previous similar antennas. The antenna maintains its performance parameters after exposure to 1.7 kGy of gamma-ray TID and TVAC cycles. According to the results of this work, the proposed antenna and materials show promise for space applications where both the RF and optical performance of the antenna should remain high. While future work, such as radiation testing beyond gamma rays, is proposed for an exhaustive environmental validation of the antenna for the space environment, the preliminary validation presented in this work suggests that the proposed antenna and materials have potential to offer a valuable new space-grade alternative for transparent solar cell integrated antennas.

Corresponding Author: Mayank – mayank@aalto.fi

Publication History: Submitted – 01/31/25; Revision Accepted – 01/13/26; Published – 05/10/26

1. Introduction

Solar cells and traditional patch antennas compete for the limited surface area of small satellite platforms (Yasin, 2013). Integrating these systems can lead to significantly more efficient utilization of the valuable spacecraft surface area (Vaccaro et al., 2003). Previously proposed solutions include directly placing solar cells on antenna patches (Vaccaro et al., 2000a, 2000b, 2001; Huang, 1998), and placing solar cells behind common antenna arrays (Huang, 1996, 1998; Maged et al., 2018). More recently, partly transparent antennas placed on top of solar cells have been proposed. The partial transparency of antennas is typically achieved either by using meshed conductor structures (Yasin et al., 2017; Turpin and Baktur, 2009; Yao et al., 2024; Ramezanzadehyazdi et al., 2022; Sun et al., 2022) or transparent conducting films (Guan et al., 2007; Hautcoeur et al., 2011b; Barato, 2023). The level of transparency of meshed conductors is limited and depends critically on the density of the mesh, which is usually composed of metals such as copper, aluminum, gold, or silver in geometrical shapes such as squares or hexagons (Jang et al., 2016; Sayem et al., 2019a; Wu et al., 2022).

Transparent films are typically based on conductive polymers, transparent conductive oxides (TCOs), or conductive inks (Gomez-Diaz and Perruisseau-Carrier, 2012). Several types of TCOs, including fluorine-doped tin oxide (FTO), aluminum zinc oxide (AZO), indium tin oxide (ITO), and gallium-doped zinc oxide (GZO) and other materials, have been explored in Syed Feroze Hussain and Thiripurasundari (2022), for example. The different conductive thin films can offer up to 90% optical transmissivity. However, the inherent trade-off between the high optical transparency achieved by thinner films is the increased sheet resistance of the films, which can degrade the RF performance of the antenna (Oubaha et al., 2012; Yasin, 2013). Previously proposed transparent antennas are typically fed through a microstrip connection that can itself be transparent, if a transparent conductive material is used.

This work proposes a solar cell-integrated antenna based on materials that present improved RF and optical performance characteristics compared to previously used materials for space antenna applications. A patch antenna prototype comprising transparent conductive carbon nanotube silver hybrid film (Chasm Advanced Materials, 2024b) and a polymethylpentene substrate (Mitsui Chemicals, 2024) is designed to operate at 4.3 GHz with a space-grade mono-crystalline silicon solar cell (Azur Space Solar Power GmbH, 2016) positioned behind it. The −10 dB impedance bandwidth of the antenna covers the frequency range from 4.1 GHz to 4.6 GHz, which includes part of the standard C-band downlink frequency range (up to 4.2 GHz) (International Telecommunication Union, 2007), as well as the frequency range dedicated to passive Earth observation satellites (4.2 GHz to 4.4 GHz) (International Telecommunication Union, 2003). While the proposed antenna prototype could be suited for both of these applications, it is not developed for any specific mission or mission requirements. The application range of the antenna can be extended further with any future prototypes by tuning the antenna element dimensions for some other frequency range.

The plastic material proposed for the prototype presents comparably low density and dielectric loss, as characterized by the low loss tangent. The conductive thin film is based on a combination of silver nanowires and carbon nanotube technology printed on a polyethylene terephthalate (PET) thin film (Chasm Advanced Materials, 2024b). The conducting film provides low sheet resistance and high optical transmissivity compared to alternatives. Moreover, it does not suffer from drawbacks associated with many alternative materials, such as the brittleness of ITO (Leppanen et al., 2013; Chen et al., 2001), and the environmental sensitivity of some conducting polymer materials (Baoyang et al., 2019). While the materials proposed in this work offer advantageous properties compared to alternatives, they have not been previously used in space antenna applications, potentially due to their prior lack of sufficient validation for the space environment.

The space-grade mono-crystalline silicon solar cells (Azur Space Solar Power GmbH, 2016) are selected for the testing of the prototype due to their

availability. This is a justified selection, as simulations show that the solar cell type does not have a significant effect on the antenna RF performance since the cell is covered by the ground plane of the antenna, which limits the interaction between the solar cell and the RF signals. Moreover, testing shows that the optical passband of the antenna covers the efficient power production wavelength range of not only silicon cells but also other cell types, such as GaAs cells. Therefore, the results of this work can be applied to similar antennas integrated to not only onto silicon but also GaAs cells that provide higher efficiency and are commonly used on space missions (Li et al., 2021).

The objective of this work is to determine the optical and RF performance of the proposed transparent solar cell integrated antenna and to preliminarily verify that the system can withstand some of the most critical environmental conditions of Earth orbit. The objective is achieved through RF and optical performance testing before and after exposure to TI gamma radiation and thermal vacuum cycling. The thermal vacuum cycling is performed following a low Earth orbit (LEO) profile. The antenna RF characteristics are determined through return loss and radiation pattern measurements, and the optical transmission properties of the antenna are measured at a dedicated facility.

The proposed antenna shows no significant RF or optical performance degradation after the environmental tests. The outgassing properties of the antenna system are also verified to comply with ECSS standards (ECSS, 2022). These results indicate promising space environment compatibility of the system. In addition, this work compares the proposed solar cell integrated antenna and its performance against previously published alternatives. The comparison reveals that the antenna of this work provides a combination of high radiation efficiency and optical transmissivity not presented by similar antennas previously, making the proposed antenna and its materials valuable options for transparent space antenna applications.

The rest of this work is structured as follows: Section 2 presents a comparison of the key performance parameters of different transparent substrate and conductor materials. Section 3 covers the design and manufacturing of the integrated solar cell antenna. Section 4 describes the measurement setups used for the RF and optical characterization, as well as TVAC and radiation testing of the antenna. In addition, the section presents the related measurement results. Section 5 discusses the results and compares the antenna presented in this work to similar previously proposed antennas. Finally, Section 6 presents the conclusions of the work.

2. Transparent Antenna Material Comparison

The PMP-type substrate material used in this work is manufactured by Mitsui Chemicals Europe GmbH with the name TPX (Mitsui Chemicals, 2024). The TPX material is selected because of its low density, low loss RF properties, and high optical transmissivity in comparison to other alternatives. Table 1 compares the mechanical and electrical properties of the substrate material with other transparent materials commonly used for transparent antennas. Additionally, the table includes two non-transparent materials (RO4003 (Hodges et al., 2017) and RT Duroid 5880 (Schmitz et al., 2025) that are typically used on satellite antennas (Abulgasem et al., 2021).

Compared to other transparent materials ranging from glass to transparent polymers, the TPX material presents lowest RF power dissipation, as shown by the lowest loss tangent. The loss tangent is used as the figure of merit for the dielectric power dissipation, as it is a typical measure provided for RF dielectrics and enables thus the comparison between the RF power losses of different materials. The RF performance parameters of the TPX material resemble closest the non-transparent RT Duroid 5880 material. The TPX material also shows lowest density of the compared options, which would assist in maintaining a low antenna system mass. The optical transparency of the material exceeds 95% for typical antenna substrate thicknesses of a few millimeters. Considering solely transparent materials covered in the comparison, only a certain type of quartz glass can achieve loss tangent values of a similar order of magnitude.

The conductive layers of transparent antennas are typically based on one of three technologies: conductive thin layers made from metal mesh films (Kang

and Jung, 2018), metal oxide films, or conductive polymers (Sayem et al., 2022).

In Table 1, loss tangent values are determined for each material at some frequency between 5 GHz to 10 GHz, since not all materials specify the loss tangent at exactly the same frequency. For the TPX material used in this work, the given loss tangent value is for 10 GHz to represent the worst-case scenario in comparison to the other materials, as the loss tangent increases with frequency for all the materials compared.

Table 2 compares typical characteristics of these conductor technologies for transparent antennas with the car-bon nanotube hybrid thin film used in this work. Whereas CNT films are typically considered to provide significantly higher sheet resistance compared to, for instance, ITO or metal mesh structures (Morimoto et al., 2023), the CNT silver hybrid film used in this work offers significantly lower sheet resistance compared to the other options. Some metal nanostructures can at best offer comparable sheet resistance, but none of the alternatives compared can provide as high optical transparency as the hybrid film used in this work. The higher conductivity and optical transparency of the CNT silver hybrid film compared to solutions using CNTs or metal mesh alone can be attributed to synergetic effects emerging from the combination of the materials (Han et al., 2017; Chasm Advanced Materials, 2024b). The optical transmission properties of CNTs also depend highly on their exact dimensions (Morimoto et al., 2014).

While the TPX substrate material used in this work has been used for ground antenna applications (Lafond et al., 2001) and it possesses some space heritage from experiments onboard the Space Shuttle (Scialdone et al., 1996), it has not been proposed for

Table 1. Transparent Substrate Material Mechanical and Electrical Properties Comparison for Antenna Applications.

Material	Type	Transparent in visible spectrum	Density (g/cm3)	Dielectric constant	Loss tangent	Space heritage	Ref.
RO4003	HCCL*	No	1.8	3.5	0.003	Yes	a, b
RT Duroid 5880	PTFE†	No	2.2	2.2	0.0009	Yes	c
SCHOTT AF 32	Glass	Yes	2.4	5.1	0.005	No	d
SCHOTT BOROFLOAT 33	Glass	Yes	2.2	4.5	0.007	Yes	d, e
SCHOTT D 263 T	Glass	Yes	2.5	6.3	0.01	No	d
Quartz glass	Glass	Yes	2.2	3.7	0.0005	Yes	f, g
PDMS	Polymer	Yes	0.97	2.8	0.07	Yes	h, i
Plexiglass	PMMA‡	Yes	1.2	3.1	0.01	Yes	j, k
Soda lime glass	Glass	Yes	-	3.1	0.02	No	l, m
PET	Polymer	Yes	1.4	2.7	0.005	Yes	n
Mitsui TPX (this work)	PMP§	Yes	0.83	2.1	0.0008	Yes	o, p

[a](Nikolaou et al., 2008), [b](Schmitz et al., 2025), [c](Rogers Corporation, 2022), [d](SCHOTT, 2018), [e](Tursuniyaz et al., 2017), [f](Hampton Research, 2016), [g](Sergeev et al., 2024), [h](Sayem et al., 2019b), [i](Lansade et al., 2020), [j](Lonsky and Hazdra, 2017), [k](Link et al., 2017), [l](Sowjanya et al., 2022), [m](Buchmayer et al., 1996), [n](Zarbakhsh et al., 2020), [o](Mitsui Chemicals, 2024), [p](Scialdone et al., 1996)
∗hydrocarbon ceramic laminate, †polytetrafluoroethylene, ‡polymethyl methacrylate, §polymethylpentene

Table 2. Conductive Layer Material Electrical and Optical Properties.

Material	Sheet resistance (Ω/sq)	Optical transparency (%)	Example	Ref.
Metal nanostructures	0.3 to 8	50 to 90	Silver nanowires	a
Metal mesh films	0.1 to 10	60 to 90	Silver, copper, gold mesh	a, b
Metal oxide films	2.5 to 25	80 to 90	ITO∗, FTO†, AZO‡, GZO§	c, d
Conductive polymers	10 to 100	90	PEDOT:PSS¶	e
Micro-metal mesh	0.05	75	-	f
CNT Film	>500	-	-	g
CNT silver hybrid film (this work)	0.2	94	AgeNT	h

[a]Naghdi et al. (2018), [b]Hautcoeur et al. (2011a), [c]Eltresy et al. (2021), [d]Sayem et al. (2020), [e]J¨onsson et al. (2003), [f] Li et al. (2017), [g]Morimoto et al. (2023), [h]Chasm Advanced Materials (2024a)
∗indium tin oxide, †fluorine-doped tin oxide, ‡aluminum zinc oxide, §gallium-doped zinc oxide, poly(3,4-ethylenedioxythiophene) polystyrene sulfonate

space antennas before. Moreover, the TPX material presents low outgassing characteristics (Walter, 1978), which is critical for space applications. Considering the advantageous electrical and optical characteristics of the substrate and conductor materials used in this work, they could represent a valuable new addition to the material options of transparent space antennas. Therefore, this work aims to determine their suitability for space antenna applications.

3. Antenna Design and Manufacturing

The antenna modeling, simulations, and optimization were carried out in CST Microwave Studio. The time do-main solver of CST was used for simulation analysis. The conductor layer was modeled as an ohmic sheet with a sheet resistance of 0.2 Ω/sq (Chasm Advanced Materials, 2024a). The solar cells were modeled as a silicon layer on an aluminum base sheet. In the simulation, the silicon material was defined to have a dielectric constant ε = 8.0 (Crovetto et al., 2017) and loss tangent tan δ = 0.0135 (Dadzadi and Pourziad, 2018). As an alternative solar cell material, GaAs (ε = 13.0 (Courtney, 2003)) was explored in simulation, with the conclusion that the solar cell type does not have a significant effect on the antenna RF performance. Due to the low thickness of the conductor layers, the meshing of the simulation model was particularly considered, and a hexahedral mesh with automatic mesh refinement provided by the CST software was used to provide sufficient mesh resolution.

The detailed stackup and dimensions of the antenna structure are illustrated in Figure 1. The stack consists of four primary layers: two conductive CNT silver hybrid film layers separated by a TPX substrate layer are placed on top of a bottom layer that is comprised of a solar cell. Other layers in the stackup are responsible for adhesion between layers (transparent adhesive and epoxy) or protection of exposed surfaces (transparent varnish). In manufacturing, layers of the 2 μm thick conductive CNT silver hybrid film are cut out in the desired shapes and attached together with PET film layers to both sides of the substrate using a transparent adhesive, and the system is coated with a transparent varnish. In the simulation, both the TPX substrate and the PET film layers were included.

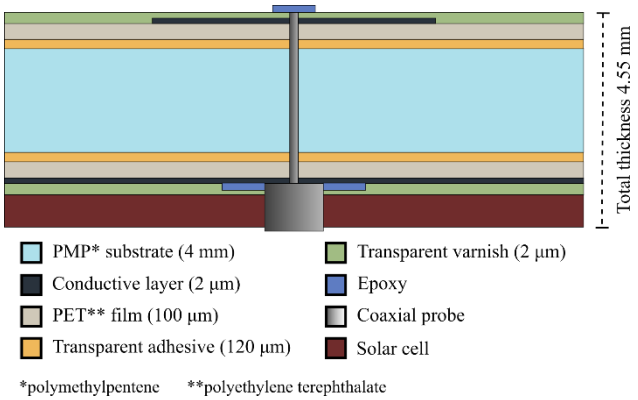

Figure 1. Stacking layout of the solar cell integrated antenna. Note: The illustrative figure is not to scale.

The mono-crystalline p-type solar cell selected for the antenna prototype presents 16.9% beginning-of-life efficiency and is designed for space applications (Azur Space Solar Power GmbH, 2016). Although other solar cell types, such as GaAs, could offer the higher efficiency often required by space missions (Li et al., 2021), silicon cells are chosen for the prototype due to their availability and comparably low cost. Moreover, based on the simulations, the selection of solar cell type is not expected to have a significant effect on the antenna RF performance, enabling the results of this work to be applied also to antennas integrated onto other types of solar cells, such as GaAs cells. Additionally, as discussed later in Section 4.2, the optical passband of the antenna covers the full wavelength range of efficient power production of also GaAs cells, making the results of this work largely applicable also to this type of cells. The 50 Ω probe feed of the patch antenna is brought through a small opening cut into the solar cell. The final dimensions of the antenna are shown in Figure 2a, and a manufactured prototype is shown in Figure 2b.

4. Antenna Testing and Verification

This section presents the testing and verification of the antenna performance. Section 4.1 discusses the impedance matching and radiation pattern test setups

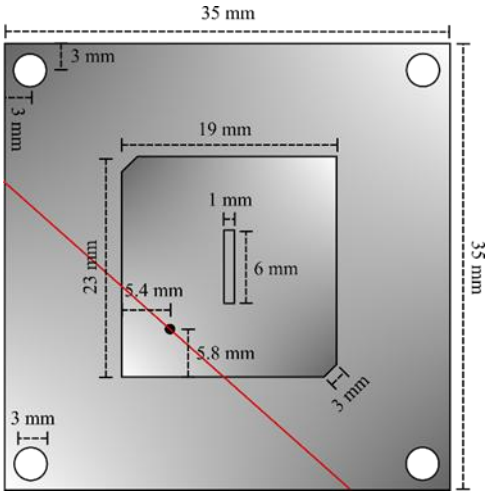

a) Antenna dimensions. The black dot represents the feed point location. The red line represents the location of the cross-section presented in Figure 1.

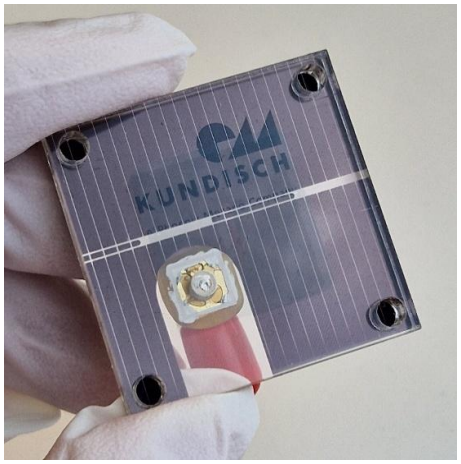

b) Manufactured hardware.

Figure 2. (a) Antenna conductor dimensions and (b) manufactured prototype hardware including the solar cell at the bottom.

and the results of tests conducted before the environmental tests. Section 4.2 describes the optical transmissivity measurement setup and the pre-environmental test results. Section 4.3 presents the environmental tests the sample antennas were exposed to. Finally, Section 4.4 shows the impedance matching and optical transmissivity measurement results obtained after the environmental tests and com-pares the results with those obtained before to evaluate the performance change caused by the TID gamma irradiation and thermal vacuum cycling.

4.1. RF Measurements

To characterize the RF performance of the antenna, its impedance matching and far field radiation pattern was measured. The impedance matching was determined through vector network analyzer (VNA) measurements. A comparison between the simulated and measured return loss of the antenna is presented in Figure 3. It should be noted that the type of solar cell does not affect the simulated performance, and the results presented here are simulated with a silicon cell. Both simulation and measurement results show satisfactory (< −10 dB) matching at the 4.3 GHz operating frequency. The double resonance peaks visible in simulation merge and appear as a single resonance peak in the measurements. This change can be attributed to differences in the parasitic capacitance and inductance of the simulated and measured antenna, arising from manufacturing-induced non-idealities. The measured −10 dB impedance bandwidth of the antenna ranges between 4.10 GHz to 4.57 GHz. This equals an absolute and relative impedance bandwidth of 470 MHz and 10.9%, respectively. At the targeted operating frequency, the matching level is −13.5 dB.

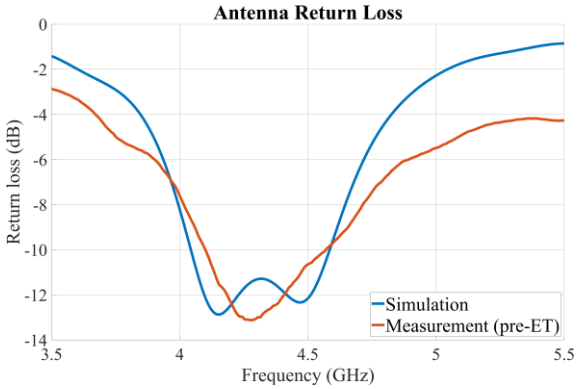

Figure 3. Simulated return loss of the solar cell integrated antenna compared to the return loss measured before the environmental testing (ET).

The far field radiation pattern of the antenna was determined by measuring the antenna radiation in the MVG Starlab 6 GHz system of Aalto University (Microwave Vision Group, 2016; Aalto University, 2024). The measurement setup in the Starlab system

is shown in Figure 4a, and two principal cuts of the radiation pattern of the antenna are presented in Figure 4b in the Starlab coordinate system ($\varphi = [0^\circ, 180^\circ]$ and $\theta = [-180^\circ, 180^\circ]$). The antenna reaches a peak gain of 8.2 dBi in the direction of $\theta = 0^\circ$, or the z-axis (see Figure 4a), and the radiation pattern is highly similar in both principal cuts. Moreover, the antenna presents a high radiation efficiency of over 81%. In future work, the relatively significant sidelobe level (approximately −4 dB) could be reduced for decreased risk of signal interference from unintended directions.

4.2. Transmissivity Measurements

The optical transmissivity measurements were performed at the Micronova facility at Aalto University using a Cary 5000 spectrometer (Caltech, 2024). Both the direct and diffuse transmissivities of the antenna were measured. Direct transmissivity is the dominant component, and the sum of the direct and diffuse transmissivities give the total transmissivity. The test setup is shown in Figure 5. In the instrument, a set of mirrors and lenses directs and collimates the test beam, and a photomultiplier tube detector measures the intensity of both the transmitted and diffused beams through the antenna.

Since a part of the antenna structure is not covered by the conductive top patch (whereas the ground plane covers the whole antenna area), the transmissivity through the antenna stack was measured from two distinct regions: a region where the top patch is included in the measured stack and another where the patch is not included. In the region with no patch, the test beam is primarily affected by the substrate and one conductive layer (the ground plane). In the region that includes the patch, the test beam is affected by the substrate and both the conductive layers (ground plane and patch). The total transmissivity of the tested antenna can be calculated by weighing the transmissivities of the two regions with their respective relative areas.

Figure 6 shows the transmissivity measurement results before environmental testing. The wavelength range of interest, 500 nm to 1000 nm, is highlighted with dashed vertical lines. This is the wavelength range where silicon solar cells primarily produce power (Strumpel et al., 2007; Green et al., 2023), and it falls within the optical passband of the antenna. In addition, it should be noted that the efficient wavelength range of also GaAs solar cells (roughly 450 nm

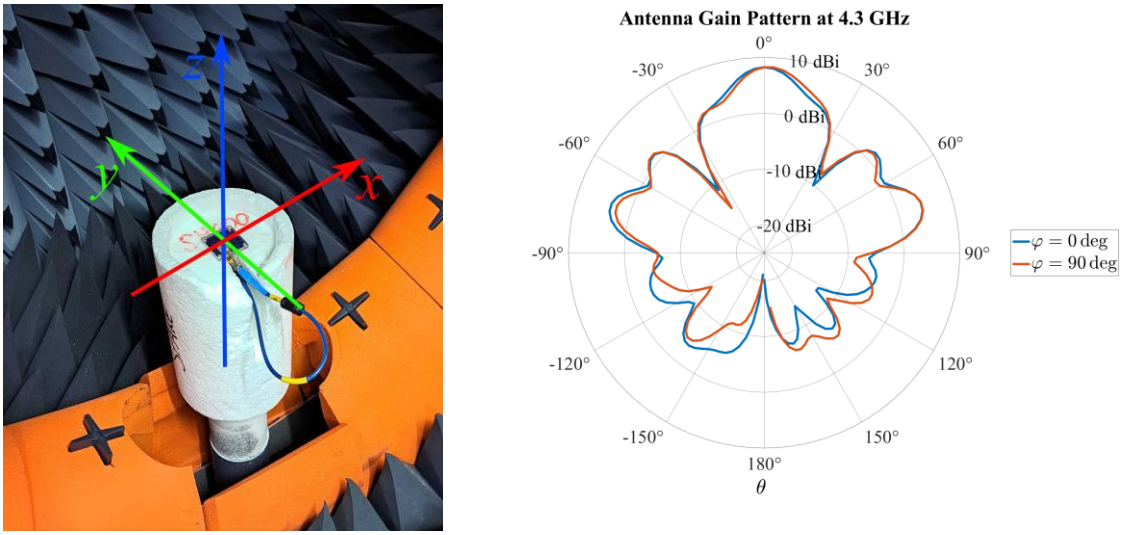

a) Radiation pattern measurement setup.

b) Principal cuts of the radiation pattern.

Figure 4. (a) Radiation pattern measurement setup in the MVG Starlab 6 GHz system. (b) Radiation pattern of the antenna. The results are presented in the non-standard spherical coordinate system used by the Starlab measurement system, i.e., $\varphi = [0^\circ, 180^\circ]$ and $\theta = [-180^\circ, 180^\circ]$. Two principal radiation pattern cuts are shown: $\varphi = 0^\circ$ in blue and $\varphi = 0^\circ$ in orange. The measurement frequency is 4.3 GHz.

Figure 5. Transmissivity test setup. The antenna is highlighted with the pink circle.

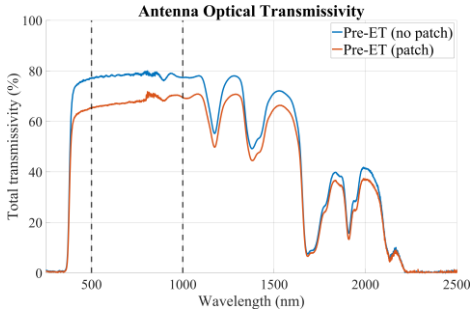

Figure 6. Total optical transmissivity of the antenna before environmental testing (ET). The transmissivity percentage is shown as a function of wavelength. Because the antenna is not completely covered by the antenna patch, the transmissivity through the antenna stack is measured from two locations: a location where the top patch is included in the measured stack (orange) and a location where the patch is not included (blue). The wavelength region of interest is between 500 nm to 1000 nm (marked with dashed black lines), the region most critical for silicon solar cell power production (Green et al., 2023).

to 850 nm (Green et al., 2022)) falls within the optical passband of the proposed antenna, enabling their use instead of silicon cells if higher solar cell efficiency is required. In the 500 nm to 1000 nm wavelength range of interest for silicon solar cells, the solar spectral power in orbit reduces towards longer wavelengths, and at 500 nm, the solar spectral power is roughly twice as high compared to 1000 nm (Xu et al., 2023). The results show that the transmissivity of the antenna in the 500 nm to 1000 nm wavelength range is between 77.0% to 80.0% in regions without the patch and between 65.2 % to 71.8 % in regions with the patch. The corresponding average transmissivities in these regions are 78.2% and 68.1%. The lower transmittance in the region covered by the patch is explained by the additional conductor sheet presented by the patch that weakens the total optical transmission through the antenna. By weighing the average transmissivities with the respective areas covered (34.4%) and not covered (65.6%) by the patch, the average optical transmissivity of the antenna is obtained to be 71.6%.

4.3. Environmental Testing

4.3.1. Gamma-Ray Irradiation

To confirm that the chosen materials do not show high sensitivity to radiation-induced degradation in optical or dielectric properties, TID testing was performed. The antenna sample was irradiated with a Co-60 gamma-ray source at a test facility of the Finnish Radiation and Nuclear Safety Authority (STUK) in Vantaa, Finland. The duration of the irradiation was 65.2 hours resulting in 1731 Gy of air kerma at the sample. A photograph of the tested sample in the measurement setup is shown Figure 7.

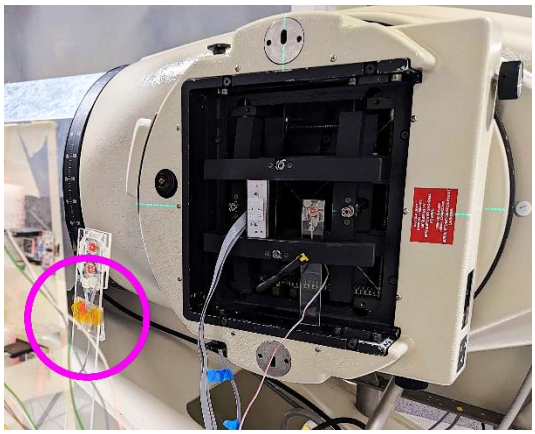

Figure 7. Gamma irradiation setup. The irradiated antenna, highlighted in pink, was placed in front of the Co-60 source together with other samples. Visible on the right is the collimator structure of the source.

It should be noted that the gamma-ray irradiation test does not represent any specific space environment. A major limitation of the Co-60 gamma rays is that they do not produce the displacement damage caused by energetic protons in space. A follow-up irradiation with a proton, neutron, or heavy ion beam would be required to qualify the sample for tolerance to displacement damage (ECSS, 2010). Moreover, the tolerance of the antenna against atomic oxygen (AO) and vacuum ultraviolet (VUV) should be quantified, as these factors can contribute to material degradation

in LEO. While the PMP substrate material used has been shown to be sensitive to AO (Scialdone et al., 1996), the PET and adhesive layers (in total over 200 μm) that cover the substrate material is expected to significantly shield the PMP material from the effects of AO that has a low penetration depth (Hansen et al., 1965; Morison et al., 1988; Zaplotnik et al., 2018). The same layers are expected to also protect the PMP material from the effects of VUV that also attenuates quickly in polymers (Fozza et al., 1999). However, conclusive evidence of the AO and VUV tolerance of the antenna can be achieved only through applicable environmental testing.

Another difference between the Co-60 gamma irradiation and the radiation environment in space is the high penetration power of the gamma rays in comparison to the low-energy electrons that dominate the particle spectra in LEO (Zyla et al., 2020; Vainio et al., 2009). These electrons are attenuated significantly by a few hundred micrometers of material, which means the dose received by the different layers of the antenna strongly depends on the layers above it, with the outer layer receiving extreme doses and the inner layer receiving modest doses. In the performed gamma-irradiation test, all layers received roughly the same dose due to the high penetration power of the gamma rays. The innermost layers, therefore, received higher doses than they would experience in space during a typical mission to LEO, while the outermost layers received a much lower dose (Donder et al., 2018).

Nevertheless, the total ionizing dose value achieved in this irradiation test has been observed to produce significant reductions in transmissivity in certain glasses (Speit et al., 1992) and measurable discolorations in polymers (Clough et al., 1996) subjected to gamma rays, which means that the test can be used to rule out heightened sensitivity of the materials to such degradation. This test can be used to determine the ability of at least the inner layers of the irradiated sample to maintain their optical transmissivity when exposed to ionizing radiation doses expected in LEO. Furthermore, the test can confirm that the chosen materials are not particularly susceptible to radiation damage.

4.3.2. Thermal Vacuum Test

To confirm that all of the materials used on the antenna can withstand the vacuum environment in space, the antenna sample was subjected to a high vacuum environment in the TVAC chamber (Nanovac TVC-800H) at Aalto University. In addition, temperature cycles based on the expected Foresail-1 LEO CubeSat environment (550 km Sun-synchronous orbit) (Palmroth et al., 2019) were applied to the test sample to confirm that typical LEO temperature range variations in a vacuum environment do not degrade the performance of the antenna. Temperature test levels were determined based on the expected maximum and minimum temperatures with additional 5◦C margins (ECSS, 2002). These levels, in addition to the selected number of five thermal cycles, comply with the definition of protoqualification testing that is sufficient to validate flight hardware for the space environment (Air Force Space Command, 2002). The TVAC test enabled also determining whether the antenna presents acceptable outgassing properties. The maximum acceptable outgassing level is determined by the ECSS standard as a total mass loss (TML) of 1.0% (ECSS, 2008).

An image of the TVAC test setup is shown in Figure 8a. The antenna samples under test were placed on stainless steel mounts on top of a copper table. The table and a shroud surrounding the test setup are the temperature-controlled elements of the chamber, and the stainless-steel mounts ensure indirect thermal contact between the table and the antennas. The heating elements of the TVAC chamber provide a nearly uniform thermal environment. The antennas remained passive throughout the TVAC test. The thermal cycles used for the test are defined in detail in Figure 8b and the accompanying Table 3. The antennas, with a low thermal mass and a thermally highly conductive connection to the temperature-controlled table, were known to follow the chamber temperature with close agreement since also the surface of the other test object that presents significantly greater thermal mass, closely followed the chamber temperature.

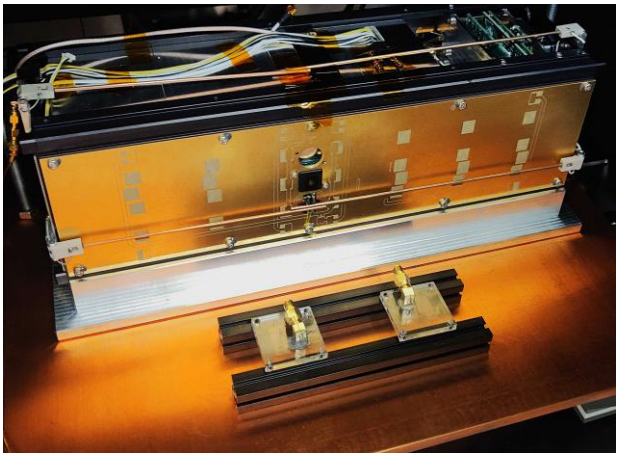

a) At the front of the picture, two transparent antenna prototypes are placed inside the thermal vacuum chamber, resting on galvanized stainless-steel mounts. Behind the antennas, an unrelated satellite is being simultaneously tested. The copper table on which the test items stand, and a surrounding shroud, are temperature controlled.

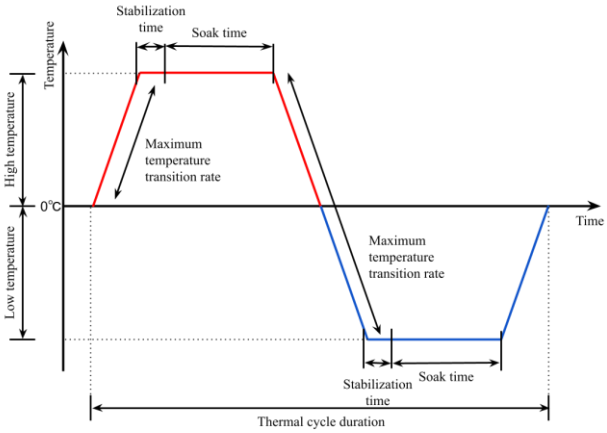

b) VAC test cycle, temperatures, cycle duration, and rate of change for non-functional test

Figure 8. (a) Thermal vacuum test setup and (b) thermal cycle parameter definitions.

Table 3: Thermal vacuum cycle parameter values. See Figure 8b for the parameter definitions

Parameter	Value	Unit
Positive temperature transition rate	2	°C/min
Negative temperature transition rate	-2	°C/min
Stabilization time	5	min
Soak time	30	min
Thermal cycle duration	155	min
Vacuum pressure	< 1 × 10-5	mbar

In addition to the five TVAC cycles, the test included a pump down and a ventilation sequence, reaching a total duration of approximately 18 hours. The maximum pressure during cycling was 1.0 × 10−5 mbar in accordance with the ECSS standard (ECSS, 2022), and the minimum pressure reached during the test was less than 1.0 × 10−6 mbar. The mass measurement of the antenna system before and after the TVAC test confirms that the outgassing properties of the antenna system is within the acceptable limit of TML < 1.0%, with a mass of 12.0 g measured both before and after the TVAC test with a measurement precision of 0.1 g. The TML result is in line with the expected low outgassing level of the substrate material (Walter, 1978). Cross-contamination risks induced by the shared-chamber testing were limited by exposing the chamber-sharing satellite to a TVAC bakeout prior to the antenna testing. In future work, collected volatile condensable material (CVCM) measurements in a TVAC environment dedicated to the antenna could be performed to more extensively characterize its outgassing properties.

4.4. Post Environmental Testing Validation

To validate the performance of the antenna after the TID gamma irradiation and thermal vacuum cycling, the RF return loss and the optical transmissivity of the antenna are remeasured. The return loss measurement can be used to validate that the electrical and RF characteristics of the antenna have not been affected (Dennison and Bray, 2020). Any notable degradation of the antenna materials can be expected to be visible as a change in the return loss measurement results compared to the measurement conducted prior to the environmental testing. The return loss measurements are performed using an HP 8720C VNA (Agilent Technologies, 1995). The return loss measurement results before and after the environmental tests, along with the estimated measurement uncertainty, is shown in Figure 9. Based on an uncertainty calculator provided by the VNA manufacturer (Keysight Technologies, 2025), the VNA measurement uncertainty is

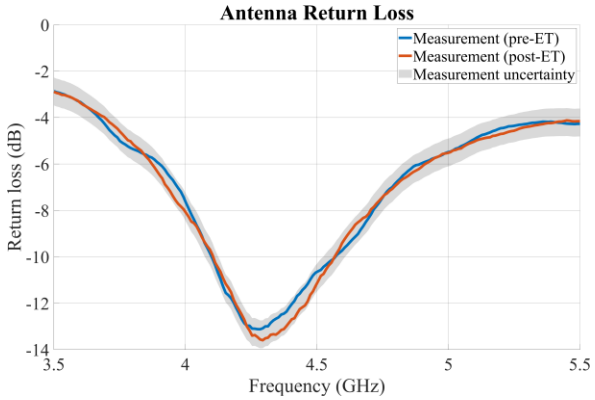

Figure 9. Measured return loss parameters of the solar cell integrated antenna before and after environmental testing (ET). The variation between measurements can be explained by the estimated ±0.6 dB uncertainty range of measurements represented by the grey area in the figure.

estimated to be ±0.6 dB. The observed differences between measurements fall within this range of uncertainty, indicating that no significant change in the antenna return loss can be identified following the environmental tests. Antenna radiation pattern measurements are not used for post environmental test verification due to the higher expected measurement uncertainty and more challenging repeatability compared to the return loss measurements.

A repeated optical transmissivity measurement is performed to evaluate the transmissivity change of the antenna. The results are compared with the transmissivity results obtained prior to the environmental tests in Figure 10. Figure 10a suggests minor transmissivity degradation at wavelengths above 800 nm for the measurement that includes the antenna patch in the stack, and Figure 10b shows the supposed transmissivity change in more detail within the wavelength region of interest (500 nm to 1000 nm). Presumably, the most notable transmissivity difference peaks can be attributed to slight wavelength offsets between the two transmissivity measurements, arising from limited measurement repeatability. This is supported by the fact that the different peaks are present only in a wavelength region where the transmissivity variation rate is high as a function of wavelength (see Figure 10a). In such regions, slight wavelength offsets can lead to peaks of one measurement and troughs of the other to align and suggest relatively major differences between the measurements even when there are none. Disregarding the most prominent peaks, the transmissivity degradation can be estimated to be at most 1% to 2% for the region with the patch.

However, the measurement results suggest even improved transmissivity of about 1% in the region without the patch (which is not expected to occur). This suggests that the measurements present accuracy and repeatability margins that could accommodate the observed changes. Furthermore, the total optical

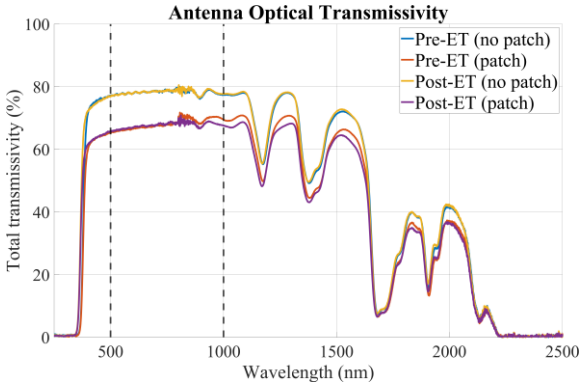

a) Total transmissivities before and after the environmental tests.

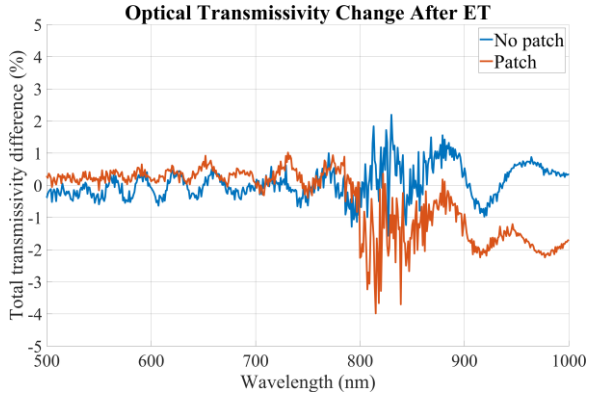

b) Transmissivity change caused by the environmental tests in the wavelength region of interest.

Figure 10. (a) Total optical transmissivity of the antenna before and after environmental testing (ET) and (b) difference between the transmissivities before and after the environmental tests. The transmissivity percentage is shown as a function of wavelength. Because the antenna is not completely covered by the antenna patch, the transmissivity through the antenna stack is measured from two locations: a location where the top patch is included in the measured stack (orange) and a location where the patch is not included (blue). The wavelength region of interest is between 500 nm to 1000 nm (marked with dashed black lines in (b)), the region most critical for silicon solar cell power production.

transmissivity change is so small that it remains 71.6%, showing no change compared to preceding results with three-digit accuracy. Therefore, while minute optical transmissivity degradation cannot be ruled out, the measurement results do not prove any definite degradation of the optical performance. However, the optical transmissivity measurement results conclusively rule out any significant radiation damage, indicating low susceptibility to gamma-induced damage.

In future work, transmissivity evaluation at off-normal incidence angles could be performed to provide transmissivity data that more comprehensively represent realistic in-orbit attitude conditions. Moreover, both return loss and transmissivity measurements could in future testing be performed following each individual stage of environmental tests to enable separately identifying any radiation or TVAC induced effects.

5. Discussion

The solar panel integrated antenna system proposed in this work presents typical patch antenna RF characteristics (Lee and Tong, 2012) with 8.2 dBi gain, 81% efficiency, and 10.9% relative bandwidth. Despite the thick (0.057 wavelengths) substrate, the antenna presents a relatively high optical transmissivity of 71.6% in the 500 nm to 1000 nm wavelength region, which is most critical for silicon solar-cell power production, as can be seen from the comparison of similar transparent C-band patch antennas presented in Table 4. The antenna proposed in this work presents one of the highest radiation efficiencies while maintaining comparably high optical transmissivity. In contrast, other similar antennas typically offer either high optical transmissivity or RF efficiency but perform significantly worse in terms of the other parameter. The better performance of the proposed antenna compared to similar alternatives can primarily be attributed to the combination of a comparably low loss, highly transparent dielectric substrate, and a conductor material that combines both one of the lowest sheet resistances and highest optical transmissivities of similar materials (see Table 2). The low losses presented by both the substrate and the conductor contribute to the radiation efficiency of the antenna, and together with a patch designed for relatively high directivity, the high radiation efficiency enables the observed comparably high gain.

The experimental results obtained from the preliminary testing of the transparent antenna under TVAC conditions and TID gamma-radiation exposure show promise regarding the space compatibility of the antenna and its materials. The return loss measurements, conducted before and after the environmental tests, do not show any significant performance change considering the estimated measurement uncertainty, indicating that the RF performance of the antenna remains unaffected by the environmental test conditions. In addition, the total mass loss of the system in the TVAC tests is verified to remain below 1.0% as required by ECSS standards, showing that the outgassing levels of the system are acceptable for space applications.

Between 800 nm to 1000 nm, optical transmissivity changes of a few percent are observed, but as discussed in Section 4.4, the results indicate that the observed differences might be at least partially attributable to measurement accuracy and repeatability limitations. Therefore, no definite conclusions about potential minor radiation-induced performance degradation can be drawn, but the results show that no major radiation damage has occurred, and the antenna system is not particularly sensitive to TID caused by gamma rays. To complete the qualification of the antenna system for the near-Earth space radiation environment, a further proton, neutron, or heavier ion beam test would be required to explore the effects of displacement damage on the materials. Nevertheless, the TID gamma-irradiation test results are promising in terms of the antenna radiation tolerance.

Since the antenna maintains a high level of optical transparency, it enables use of surface area previously occupied exclusively by antennas also for solar cell power generation purposes. As the power P generated

Table 4. Thermal Vacuum Cycle Parameter Values. See Figure 8b for the parameter definitions.

Ref.	Freq. (GHz)	Substrate	Conductor	Thick-ness (mm)	Gain (dBi)	Rad. Eff. (%)	Band-width (%)	Transmissiv-ity (%)
a	5.8	Soda lime glass	AgITO*	1.1	5.0	56.6	8.0	-
b	4.7-5.6	PDMS†	Metal mesh	3.0	3.1	46.0	13.6	50-70
c	5.8	Glass	ITO‡	1.0	6.0	-	2.2	-
d	5	Pyrex Glass	FTO§	4.0	3.6	50-67	12.0	72-84
e	4.9	Soda lime glass	FTO§	4.4	5.2	82.0	16.3	60.0
f	3.4	PDMS†	EGaIn¶	3-4	3.5	60.0	1.2	-
g	5.15-5.8	Glass	MMMC‖ film	1.1	2.3	46.0	4.3	75.0
h	5	Borosilicate glass	ITO‡ / copper	1.3	2.2	67.0	-	55.0
This work	**4.3**	**TPX (PMP**)**	**CNT†† silver hybrid film**	**4.6**	**8.2**	**81.0**	**10.9**	**71.6**

[a]Eltresy et al. (2021), [b]Sayem et al. (2019a), [c]Yao et al. (2017), [d]Sheikh et al. (2015), [e]Sowjanya et al. (2022), [f]Hayes et al. (2012), [g]Li et al. (2017), [h]Haraty et al. (2016) *silver indium tin oxide, †polydimethylsiloxane, ‡indium tin oxide, §fluorine-doped tin oxide, ¶eutectic gallium-indium, ‖micro-metal mesh conductor, **polymethylpentene, ††carbon nanotube

by a solar cell is directly proportional to the solar flux density S (i.e., $P \propto S$) (Wertz et al., 2011), the 28.4 % optical absorption decreases the power production capacity of the solar cell by an equal amount. However, when comparing to an antenna without a solar cell, the solar cell integrated antenna provides significant additional power generation potential. Furthermore, as the antenna adds more material on top of the solar cell, it can offer some level of radiation shielding to the cell, thus reducing the long-term degradation of its power generation capacity (Messenger et al., 2010). The results of this work suggest that the proposed materials can provide a new option for transparent antenna applications with a specific balance between RF and optical performance not provided previously by existing alternatives. The combination of high RF efficiency and optical transmissivity, together with low substrate density that reduces the antenna mass, can also be considered favorable for space applications. While more extensive and comprehensive environmental testing is proposed for the future, the preliminary environmental test results presented in this work show encouraging first results in terms of tolerance to the space environment.

In future work, tests could be performed for a larger sample batch to enable statistical insight that allows reducing test result uncertainty that arises from measurement repeatability limitations caused, for instance, by measurement setup fixture tolerances and calibration uncertainties. Radiation tests could be performed at multiple levels to enable interpolation and the demonstration of margins. Testing should also be extended by proton, neutron, or heavy ion beam irradiation to quantify effects of displacement damage, and testing in VUV and AO environments should be considered. Moreover, qualification level TVAC testing would further qualify the antenna for the relevant space environment, and CVCM measurement would

provide more detailed information about the outgassing properties of the antenna system. Separating the potential effects of TVAC and different types of radiation tests could be achieved by exposing selected antenna units to only one of the environmental test types. These considerations would enable future research to build upon the promising results of this work.

6. Conclusion

This work presents the design of a transparent solar cell integrated C-band patch antenna based on materials not previously proposed for transparent space antenna applications. The materials used (Mitsui TPX PMP substrate and a conductive CNT silver hybrid film) were chosen due to their low RF loss properties and high optical transmissivity compared to previously proposed alternative materials, which makes them lucrative options for high-performance transparent antennas. Furthermore, this work tests and validates the proposed antenna and its materials for space applications through a preliminary environmental test campaign comprised of TVAC cycling following a LEO profile and TID gamma irradiation.

The proposed antenna presents a −10 dB impedance bandwidth of nearly 11%, a gain exceeding 8 dBi, and a radiation efficiency of 81% at the designed operating frequency of 4.3 GHz. In addition, the antenna system presents high optical transmissivity (71.6%) compared to similar alternative antennas in the wavelength region most important for silicon solar cell power production. The proposed antenna provides a balance between radiation efficiency and optical transmissivity not previously presented by similar antennas, which can enable simultaneously satisfying both stringent RF and optical performance requirements. Moreover, the RF performance of the antenna, characterized by the return loss, is not significantly affected by the environmental tests considering the measurement precision limits. The minor changes observed in optical transmissivity can likely also be primarily attributed to measurement repeatability limitations. The outgassing level of the antenna is shown through TML characterization to remain within acceptable limits.

According to the results of this work, the antenna and its materials show encouraging promise for space applications. For full confidence, a follow-up irradiation with, for example, a proton beam would be required to qualify the sample for tolerance to displacement damage, since this cannot be observed with TID gamma-ray irradiation. Also, the tolerance of the antenna against VUV and AO should be quantified in future test campaigns. Additionally, full qualification level TVAC testing should be performed, and CVCM measurements should be considered. For reduced measurement uncertainty, a larger quantity of samples could be tested, and different batches of antenna units could be exposed to different types of environmental tests to enable separating the potential effects induced by different types of radiation exposure and TVAC cycling. Nevertheless, this work presents a clear preliminary indication that the proposed antenna and transparent materials could potentially offer a valuable alternative for existing transparent antenna technologies in space, enabling more efficient use of small spacecraft surface area.

Acknowledgments

The project was conducted with the support of Celestial Space Technologies GmbH, Germany. Antenna manufacturing was performed by Kundisch GmbH & Co. KG. Antenna testing was carried out at Aalto University, Finland.

References

Aalto University (2024): Aalto University Starlab. Available at: https://www.aalto.fi/en/department-of-electronics-and-nanoengineering/aalto-electronics-ict#3-starlab (accessed Aug. 22, 2024).

Abulgasem, S., Tubbal, F., Raad, R., Theoharis, P. I., Lu, S. and Iranmanesh, S. (2021): Antenna Designs for Cubesats: A Review. IEEE Access, Vol. 9, pp. 45289–45324. doi: 10.1109/ACCESS.2021.3066632.

Agilent Technologies (1995): 8719C, 8720C, 8722A/C Network Analyzer Operating Manual.

Available at: https://www.keysight.com/us/en/assets/9018-05168/user-manuals/9018-05168.pdf (accessed Oct. 20, 2025).

Air Force Space Command (2002): SMC Standard SMC-S-016 - Test Requirements for Launch, Upper-Stage and Space Vehicles.

Azur Space Solar Power GmbH (2016): Silicon Solar Space Cell s32. Available at: https://www.azurspace.com/en/products/space-products/ (accessed Oct. 6, 2025).

Baoyang, L., Hyunwoo, Y., Shaoting, L., Nannan, J., Kai, Q., Jingkun, X. and Zhao, X (2019): Pure Pedot: Pss Hydrogels. Nature Communications, Vol. 10, p. 1043. Available at: https:// www.nature.com/articles/s41467-019-09003-5 (accessed Aug. 22, 2024). doi: 10.1038/s41467-019-09003-5.

Barato, F. (2023): Optimal Use of Electric Propulsion for Drag Compensation in Very Low Earth Orbit on Satellites with Deployable Solar Panels. Acta Astronautica, Vol. 213, pp. 1–19. doi: 10.1016/j.actaastro.2023.08.038.

Buchmayer, G., Rädlein, E., Frischat, G., Beier, W. and Speit, B. (1996): Paramagnetic Centers in Glasses Induced by Low Earth Orbit Space Radiation. J. of Non-crystalline Solids, Vol. 204, No. 3, pp. 253–259.

Caltech (2024): User Guide for Cary 5000 Spectrometer with External Dra 1800 Attachment. Available at: https://mmrc.caltech.edu/Cary% 20UV-Vis%20Int.Sphere/manuals/Cary5000_ User_Guide.pdf (accessed Jan. 3, 2024).

Chasm Advanced Materials (2024a): Agent G3 Datasheet. Available at: https://www.chasmtek.com/hubfs/Documents/Datasheets/ (%20TDS%20)%20AgeNT-1%20-%20G3.pdf (accessed Aug. 22, 2024).

Chasm Advanced Materials (2024b): Agent Transparent Conductive Films. Available at: https://www.chasmtek.com/agent-overview (accessed Aug. 22, 2024).

Chen, Z., Cotterell, B., Wang, W., Guenther, E. and Chua, S.-J. (2001): A Mechanical Assessment of Flexible Optoelectronic Devices. Thin Solid Films, Vol. 394, No. 1, pp. 201–205. Available at: https://www.sciencedirect.com/science/article/pii/S0040609001011385 (accessed Aug. 22, 2024). doi: 10.1016/S0040-6090(01)01138-5. ISSN 0040-6090.

Clough, R., Gillen, K., Malone, G. and Wallace, J. (1996): Color Formation in Irradiated Polymers. Radiation Physics and Chemistry, Vol. 48, No. 5, pp. 583–594. Available at : https://www.sciencedirect.com/science/article/pii/0969806X 96000758 (accessed Aug. 22, 2024). doi: 10.1016/0969-806X(96)00075-8. ISSN 0969-806X.

Courtney, W. E. (2003): Complex Permittivity of GaAs and CdTe at Microwave Frequencies. IEEE Trans. on Microwave Theory and Techniques, Vol. 25, No. 8, pp. 697–701.

Crovetto, A., Huss-Hansen, M. K. and Hansen, O. (2017): How the Relative Permittivity of Solar Cell Materials Influences Solar Cell Performance. Solar Energy, Vol. 149, pp. 145–150. doi: 10.1016/j.solener.2017.04.018.

Dadzadi, A. and Pourziad, A. (2018): A Novel X-band Circular Polarized Reflectarray Element Integrated with Solar Cells, in Proc. Iranian Conf. on Electrical Engineering (ICEE), pp. 446–451. doi: 10.1109/ICEE.2018.8472680.

Dennison, J. R. and Bray, M. G. (2020): Radial Line Slot Array Antenna High Power Thermal Vacuum Testing, in 2020 IEEE Int. Symp. on Antennas and Propagation and North American Radio Science Mtg, pp. 257–258. doi: 10.1109/IEEECONF 35879.2020.9330261.

Donder, E. D., Messios, N., Calders, S. et al. (2018): SPace ENVironment Information System: SPENVIS. Available at: https://www.spenvis.oma.be/ (accessed Oct. 6, 2025).

ECSS (2002): ECSS-E-10-03A - Space Engineering - Testing. Available at: https://ecss.nl/standard/ ecss-e-10-03a-testing/ (accessed Apr. 18, 2025).

ECSS (2008): ECSS-q-st-70-02c - Thermal Vacuum Outgassing Test for the Screening of Space Materials. Available at: https://ecss.nl/standard/ ecss-q-st-70-02c-thermal-vacuum-outgassing-test-for-the-screening-of-space-materials/ (accessed Mar. 12, 2025).

ECSS (2010): ECSS-E-HB-10-12A - Calculation of Radiation and its Effects and Margin Policy Handbook. Available at: https://ecss.nl/hbstms/ ecss-e-

hb-10-12a-calculation-of-radiation-and-its-effects-and-margin-policy-handbook/ (Apr. 18, 2026).

ECSS (2022): ECSS-e-st-10-03c rev.1 – Testing. Available at: https://ecss.nl/standard/ecss-e-st-10-03c-rev-1-testing-31-may-2022/ (accessed Jan. 1, 2025).

Eltresy, N. A., Elhamid, A. E. M. A., Elsheakh, D. M., Elhennawy, H. M. and E. A. Abdallah, E. A. (2021): Silver Sandwiched ito Based Transparent Antenna Array for rf Energy Harvesting in 5g Mid-range of Frequencies. IEEE Access, 9:49476–49486. doi: 10.1109/ACCESS.2021.3069409.

Fozza, A., Klemberg-Sapieha, J. and Wertheimer, M. R. (1999): Vacuum Ultraviolet Irradiation of Polymers. Plasmas and Polymers, Vol. 4, No. 2, pp. 183–206.

Gomez-Diaz, J. S. and Perruisseau-Carrier, J. (2012): Microwave to THz Properties of Graphene and Potential Antenna Applications, in 2012 Int. Symp. on Antennas and Propagation (ISAP), pp. 239–242. IEEE. ISBN 978-4-88552-270-3.

Green, M. A., Dunlop, E. D., Hohl-Ebinger, J., Yoshita, M., Kopidakis, N., Bothe, K., Hinken, D., Rauer, M. and Hao, X. (2022): Solar Cell Efficiency Tables (Version 60), Progress in Photovoltaics, Vol. 30, No. 7.

Green, M. A., Dunlop, E. D., Siefer, G., Yoshita, M., Kopidakis, N., Bothe, K. and Hao, X. (2023): Solar Cell Efficiency Tables (Version 61), Progress in Photovoltaics: Research and Applications, Vol. 31, No. 1, pp. 3–16. Available at: https://onlinelibrary.wiley.com/doi/abs/-10.1002/pip.3646. doi: https://doi.org/10.1002/ pip.3646.

Guan, N., Furuya, H., Himeno, K., Goto, K. and Ito, K. (2007): Basic Study on an Antenna Made of a Transparent Conductive Film. IEICE Trans. on Comms., Vol. 90, No. 9, pp. 2219–2224. doi: 10.1093/ietcom/e90-b.9.2219.

Hampton Research (2016): Quartz-glass. Available at: https://hamptonresearch.com/uploads/-support_materials/Quartz_Capillary_Technical_Data_Sheet.pdf (accessed Jan. 3, 2024).

Han, Y., Liu, Y., Han, L., Lin, J. and Jin, P. (2017): High-performance Hierarchical Graphene/metal-mesh Film for Optically Transparent Electromagnetic Interference Shielding. Carbon, Vol. 115, pp. 34–42.

Hansen, R., Pascale, J., De Benedictis, T. and Rentzepis, P. (1965): Effect of Atomic Oxygen on Polymers. J. of Polymer Science Part A: General Papers, Vol. 3, No. 6, pp. 2205–2214.

Haraty, M. R., Naser-Moghadasi, M., Lotfi-Neyestanak, A. A. and Nikfarjam, A. (2016): Improving the Efficiency of Transparent Antenna Using Gold Nanolayer Deposition. IEEE Antennas and Wireless Propagation Letters, Vol. 15, pp. 4–7. doi: 10.1109/LAWP.2015.2424918.

Hautcoeur, J., Castel, X., Colombel, F., Benzerga, R., Himdi, M., Legeay, G. and Motta-Cruz, E. (2011a): Transparency and Electrical Properties of Meshed Metal Films. Thin Solid Films, Vol. 519, No. 11, pp. 3851–3858.

Hautcoeur, J., Colombel, F., Castel, X., Himdi, M. and Cruz, E. M. (2011b): Radiofrequency Performances of Transparent Ultra-wideband Antennas. Progress In Electromagnetics Research C, Vol. 22, pp. 259–271. doi: 10.2528/ PIERC11052606.

Hayes, G. J., So, J.-H., Qusba, A., Dickey, M. D. and Lazzi, G. (2012): Flexible Liquid Metal Alloy (egain) Microstrip Patch Antenna. IEEE Trans. on Antennas and Propagation, Vol. 60, No. 5, pp. 2151–2156. doi:10.1109/TAP.2012.2189698.

Hodges, R. E., Chahat, N., Hoppe, D. J. and Vacchione, J. D. (2017): A Deployable High-gain Antenna Bound for Mars: Developing a New Folded-panel Reflectarray for the First Cubesat Mission to Mars. IEEE Antennas and Propagation Magazine, Vol. 59, No. 2, pp. 39–49. doi: 10.1109/MAP.2017.2655561.

Huang, J. (1996): Capabilities of Printed Reflectarray Antennas, in Proc. of Int. Symp. on Phased Array Systems and Technology, pp. 131–134. IEEE. doi: 10.1109/PAST.1996.565950.

Huang, J. (1998): Mars Rover Antenna for Solar-array Integration. Telecommun. Mission Oper. Prog. Rep, 42:136. Available at: https://ipnpr.jpl.nasa.gov/progress_report/42-136/136C.pdf (accessed Aug. 22, 2024).

International Telecommunication Union. Rec. ITU-R RS.1624 (2003): Available at: https://www.

itu.int/dms_pubrec/itu-r/rec/rs/R-REC-RS.1624-0-200305-I!!PDF-E.pdf (accessed Oct. 6, 2025).

International Telecommunication Union. Rep. ITU-R M.2109 (2007): Available at: https://www.itu.int/dms_pub/itu-r/opb/rep/R-REP-M.2109-2007-PDF-E.pdf (accessed Oct. 6, 2025).

Jang, T., Zhang, C., Youn, H., Zhou, J. and Guo, L. J. (2016): Semitransparent and Flexible Mechanically Reconfigurable Electrically Small Antennas Based on Tortuous Metallic Micromesh. IEEE Trans. on Antennas and Propagation, Vol. 65, No. 1, pp. 150–158. doi: 10.1109/TAP.2016.2623479.

Jönsson, S., Birgerson, J., Crispin, X., Greczynski, G., Osikowicz, W., Denier van der Gon, A., Salaneck, W. and Fahlman, M. (2003): The Effects of Solvents on the Morphology and Sheet Resistance in Poly(3,4-ethylenedioxythiophene)–polystyrenesulfonic Acid (pedot–pss) Films. Synthetic Metals, Vol. 139, No. 1, pp. 1–10. Available at: https://www.sciencedirect.com/science/article/pii/S0379677902012596 (accessed Aug. 22, 2024). doi: 10.1016/S0379-6779(02)01259-6. ISSN: 0379-6779.

Kang, S. H. and Jung, C. W. (2018): Transparent Patch Antenna Using Metal Mesh. IEEE Trans. on Antennas and Propagation, Vol. 66, No. 4, pp. 2095–2100. doi: 10.1109/TAP.2018.2804622.

Keysight Technologies (2025): Downloadable Vector Network Analyzer Uncertainty Calculator. Available at: https://www.keysight.com/us/en/lib/ software-detail/computer-software/downloadable-vector-network-analyzer-uncertainty-calculator-1000000418epsgsud.html (accessed Oct. 6, 2025).

Lafond, O., Himdi, M. and Daniel, J. (2001): Thick Slot-coupled Printed Antenna Arrays for a 60 ghz Indoor Communication System. Microwave and Optical Technology Letters, Vol. 28, No. 2, pp. 105–108.

Lansade, D., Lewandowski, S., Remaury, S., Sierra, G., Solé, S., Perraud, S. and Carlotti, S. (2020): Enhanced Resistance to Proton Irradiation of Poly(dimethylsiloxane) Resins Through Surface Embedding of Silica Photonic Crystals. Polymer Degradation and Stability, Vol. 176, p. 109163. Available at: https://www.sciencedirect.com/ science/article /pii/S0141391020300951 (accessed Aug. 22, 2024). doi: https://doi.org/10.1016/j.polymdegradstab.2020-.109163. ISSN 0141-3910.

Lee, K.-F. and Tong, K.-F. (2012): Microstrip Patch Antennas—Basic Characteristics and Some Recent Advances, in Proc. of the IEEE, Vol. 100, No. 7, pp. 2169–2180.

Leppänen, K., Augustine, B., Saarela, J., Myllylä, R. and Fabritius, T. (2013): Breaking Mechanism of Indium Tin Oxide and its Effect on Organic Photovoltaic Cells. Solar Energy Materials and Solar Cells, Vol. 117, pp. 512–518. Available at: https://www.sciencedirect.com/science/article/pii/S0927024813003565 (accessed Aug. 22, 2024). doi: 10.1016/j.solmat.2013.07.010. ISSN 0927-0248.

Li, J., Aierken, A., Liu, Y., Zhuang, Y., Yang, X., Mo, J., Fan, R., Chen, Q., Zhang, S., Huang, Y. et al. (2021): A Brief Review of High Efficiency iii-v Solar Cells for Space Application. Frontiers in Physics, Vol. 8, p. 631925.

Li, Q. L., Cheung, S. W., Wu, D. and Yuk, T. I. (2017): Optically Transparent Dual-band Mimo Antenna Using Micro-metal Mesh Conductive Film for wlan System. IEEE Antennas and Wireless Propagation Letters, Vol. 16, pp. 920–923. doi: 10.1109/ LAWP.2016.2614577.

Link, S., Huang, X., Fernandez-Pello, C. et al. (2017): The Effect of Gravity on Flame Spread Over pmma Cylinders. Scientific Repts. doi: 10.1038/s41598-017-18398-4.

Lonsky, T. and Hazdra, P. (2017): Design of a Plexiglass Rod Antenna, in 2017 Conf. on Microwave Techniques (COMITE), pp. 1–5. doi: 10.1109/COMITE.2017.7932300.

Maged, M. A., Elhefnawi, F., Akah, H. M. and El-Hennawy. H. M. (2018): C-band Transparent Antenna Design for Intersatellites Communication. Int. J. of Scientific & Engineering Research, Vol. 9, No. 3, pp. 248–252.

Messenger, S., Jackson, E., Warner, J. and Walters, R. (2010): Scream: A New Code for Solar Cell Deg-

radation Prediction Using the Displacement Damage Dose Approach, in 2010 Proc. 35th IEEE Photovoltaic Specialists Conf., pp. 001106–001111.

Microwave Vision Group (2016): Antenna Measurement and Radome Test Systems. Available at: https://www.rftest.co.nz/assets/ Downloads/Accessible/MVG/2952f6a8be/MVG-Antenna-Measurement.pdf (accessed Oct. 20, 2025).

Mitsui Chemicals (2024): Tpx Datasheet. Available at: https://jp.mitsuichemicals.com/en/special/tpx/properties_table/ (accessed Aug. 22, 2024).

Morimoto, T., Joung, S.-K., Saito, T., Futaba, D. N., Hata, K. and Okazaki, T. (2014): Length-dependent Plasmon Resonance in Single-walled Carbon Nanotubes. ACS nano, Vol. 8, No. 10, pp. 9897–9904.

Morimoto, Y., Shiu, S., Huang, I. W., Fest, E., Ye, G. and Zhu, J. (2023): Optically Transparent Antenna for Smart Glasses. IEEE Open J. of Antennas and Propagation, Vol. 4, pp. 159–167.

Morison, W., Tennyson, R., French, J., Braithwaite, T., Moisan, M. and Hubert, J. (1988): Atomic Oxygen Studies on Polymers, in Proc. 15th Space Simulation Conf.: Support the Highway to Space Through Testing. NASA, Goddard Space Flight Center, MD.

Naghdi, S., Rhee, K. Y., Hui, D. and Park, S. J. (2018): A Review of Conductive Metal Nanomaterials as Conductive, Transparent, and Flexible Coatings, Thin Films, and Conductive Fillers: Different Deposition Methods and Applications. Coatings, Vol. 8, No. 8, p. 278. Available at: https://www.mdpi.com/2079-6412/8/8/278 (accessed Aug. 22, 2024). doi: 10.3390/coatings8080278. ISSN 2079-6412.

Nikolaou, S., Vryonides, P. and Anagnostou, D. E. (2008): Dual-band Microstrip-fed Monopole on ro4003 Substrate, in 2008 IEEE Proc., Int'l. Symp. Antennas and Propagation Society, pp. 1–4. doi:10.1109/APS.2008.4619886.

Oubaha, M., Elmaghrum, S., Copperwhite, R., Corcoran, B., McDonagh, C. and Gorin, A. (2012): Optical Properties of High Refractive Index Thin Films Processed at Low-temperature. Optical Materials, Vol. 34, No. 8, pp. 1366–1370. Available at: https://www.sciencedirect.com/ science/article/ pii/S0925346712000948 (accessed Sept. 4, 2025). doi: 10.1016/j.optmat.2012.02. 023. ISSN 0925-3467.

Palmroth, M., Praks, J., Vainio, R., Janhunen, P., Kilpua, E., Afanasiev, A., Ala-Lahti, M., Alho, A., Asikainen, T., Asvestari, E. et al. (2019): Foresail-1 Cubesat Mission to Measure Radiation Belt Losses and Demonstrate Deorbiting. J. of Geophysical Research: Space Physics, Vol. 124, No. 7, pp. 5783–5799.

Ramezanzadehyazdi, S., Shafai, C., Isleifson, D., Shafai, L. and Ferguson, P. (2022): An Optically Transparent Meshed Patch Antenna with Enhanced Bandwidth for Cubesat Applications, in 2022 Proceedings, IEEE Int. Conf. on Wireless for Space and Extreme Environments (WiSEE), pp. 44–48.

Rogers Corporation (2022): Rt Duroid 5880. Available at : https://rogerscorp.com/-/media/project/rogerscorp/documents/advanced-electronics-solutions/english/data-sheets/rt-duroid-5870---5880-data-sheet.pdf (accessed Jan. 2, 2024).

Sayem, A. S. M., Simorangkir, R. B., Esselle, K. P. and Hashmi, R. M. (2019a): Development of Robust Transparent Conformal Antennas Based on Conductive Mesh-polymer Composite for Unobtrusive Wearable Applications. IEEE Trans. on Antennas and Propagation, Vol. 67, No. 12, pp. 7216–7224. doi: 10.1109/TAP.2019.2930116.

Sayem, A. S. M., Simorangkir, R. B. V. B., Esselle, K. P. and R. M. Hashmi, R. M. (2019b): Development of Robust Transparent Conformal Antennas Based on Conductive Mesh-polymer Composite for Unobtrusive Wearable Applications. IEEE Trans. on Antennas and Propagation, Vol. 67, No. 12, pp. 7216–7224. doi: 10.1109/TAP.2019.2930116.

Sayem, A. S. M., Simorangkir, R. B., Esselle, K. P., Hashmi, R. M. and Liu, H. (2020): A Method to Develop Flexible Robust Optically Transparent Unidirectional Antennas Utilizing Pure Water, PDMS, and Transparent Conductive Mesh. IEEE Trans. on Antennas and Propagation, Vol. 68, No. 10, pp. 6943–6952.

Sayem, A. S. M., Lalbakhsh, A., Esselle, K. P., Buckley, J. L., O'Flynn, B. and R. B. V. B. Simorangkir, R. B. V. B. (2022): Flexible Transparent Antennas: Advancements, Challenges, and Prospects. IEEE Open J. of Antennas and Propagation, Vol. 3, pp. 1109–1133. doi: 10.1109/OJAP.2022.3206909.

Schmitz, L. K., Pedivellano, A., van Leusen, W., Taas, N., Gruber, J., Sinn, T., Schumacher, J., Mayank., Banea, K., Panzer, S. et al. (2025): Development of the Maras 1-m2 ka-band Deployable Reflectarray Antenna, in Proc. AIAA SCITECH 2025 Forum, p. 1408. Available at: https://arc.aiaa.org/doi/abs/10.2514/ 6.2025-1408 (accessed Jan. 22, 2025). doi: 10.2514/6.2025-1408.

SCHOTT (2018): Electrical Properties of SCHOTT Thin Glasses. Available at: https://www.schott.com/en-dk/products/d-263/-/media/project/onex/products/d/d263/downloads/row-schott-electrical-properties-datenflyer-view-2019-05-24.pdf (accessed Jan. 2, 2024).

Scialdone, J. J., Clatterbuck, C. H., Ayres-Treusdell, M., Park, G. and Kolos, D. (1996): Atomic Oxygen and Space Environment Effects on Aerospace Materials Flown with EOIM-3 Experiment. NASA Tech. Rept. NASA-TM-104636. Available at: https://ntrs.nasa.gov/archive/nasa/casi.ntrs. nasa.gov/19970010450.pdf (accessed Aug. 19, 2025).

Sergeev, V. P., Tursunkhanova, R. B., Kalashnikov, M. P., Sergeev, O. V., Voronov, A. V. and Neyfeld, V. V. (2024): The Peculiar Alterations of the Optical and Mechanical Characteristics of the Quartz Glass Plates with a Reinforcing Coating Under the Collision with a Hyper-velocity Flux of Microparticles. Acta Astronautica, Vol. 216, pp. 428–436. Available at: https://www.sciencedirect.com/science/article/pii/S0094576524000316 (accessed Aug. 22, 2024). doi: https://doi.org/10.1016/j.actaastro.2024.01.025. ISSN 0094-5765.

Sheikh, S., Shokooh-Saremi, M. and Bagheri-Mohagheghi, M.-M. (2015): Transparent Microstrip Patch Antenna Based on Fluorine-doped Tin Oxide Deposited by Spray Pyrolysis Technique. IET Microwaves, Antennas & Propagation, Vol. 9, No. 11, pp. 1221–1229. doi: 10.1049/iet-map.2015.0048.

Sowjanya, P. D., Alsath, M. G. N., Kirubaveni, S., Govindaraj, R. and Santhosh, N. (2022): Design and Experimental Evaluation of a Proximity Coupled Transparent Patch Antenna for WLAN. IETE J. of Research, Vol. 68, No. 1, p. 77–84. doi: 10.1080/03772063.2019.1588174.

Speit, B., Rädlein, E., Frischat, G. H., Marker, A. J. and Hayden, J. S. (1992): Radiation Resistant Optical Glasses. Nuclear Instruments and Methods in Physics Research Section B: Beam Interactions with Materials and Atoms, Vol. 65, Nos. 1-4, pp. 384–386. doi: 10.1016/0168-583X(92)95071-X.

Strumpel, C., McCann, M., Beaucarne, G., Arkhipov, V., Slaoui, A., Švrček, V., del Cañizo, C. and Tobias, I. (2007): Modifying the Solar Spectrum to Enhance Silicon Solar Cell Efficiency—An Overview of Available Materials. Solar Energy Materials and Solar Cells, Vol. 91, No. 4, pp. 238–249. Available at: https://www.sciencedirect.com/ science/article/pii/-S0927024806003679 (accessed Aug. 22, 2024). doi: 10.1016/j.solmat.2006.09.003. ISSN 0927-0248.

Sun, X.-T., Zhao, Q., Lu, W.-Z. and Wang, X.-C. (2022): Optical Transparent Broadband Antenna Array Integrated with Polycrystalline Silicon Solar Cells. IEEE Antennas and Wireless Propagation Letters, Vol. 22, No. 2, pp. 248–252.

Syed Feroze Hussain, S. and Thiripurasundari, D. (2022): A Review on Optically Transparent Antenna Fabricated with Conductive Nano-material Oxides. J. of Electronic Materials, Vol. 51, No. 12, pp. 6707–6734. doi: 10.1007/s11664-022-09916-w.

Turpin, T. W. and Baktur, R. (2009): Meshed Patch Antennas Integrated on Solar Cells. IEEE Antennas and Wireless Propagation Letters, Vol. 8, pp. 693-696. doi: 10.1109/LAWP.2009. 2025522.

Tursuniyaz, M., Martineau, R., Baktur, R., Swenson, C., Altunc, S., Onuma, E., Shelton, M. and Shaw, H. (2017): A Clear Antenna on Cubesat for Big Data, in Proc. AIAA/USU Conf. on Small Satellites, Logan, UT. Available at: https://digitalcom-

mons.usu.edu/smallsat/2017/all2017/75/ (accessed Oct. 15, 2025). Also available as NASA Tech. Memorandum NASA/TM-2017-219682.

Vaccaro, S., Torres, P., Mosig, J., Shah, A., Skrivervik, A., Zürcher, J., de Maagt, P. and Gerlach, L. (2000a): Integration of Antennas and Solar Cells for Satellite Communications, in Proc. AP2000 Millenium Conf. on Antennas & Propagation, pp. 1–4.

Vaccaro, S., Torres, P., Mosig, J., Shah, A., Zürcher, J., Skrivervik, A., Gardiol, F., De Maagt, P. and Gerlach, L. (2000b): Integrated Solar Panel Antennas. Electronics Letters, Vol. 36, No. 5, pp. 390–391. doi: 10.1049/el:20000350.

Vaccaro, S., Torres, P., Mosig, J., Shah, A., Skrivervik, A., Zürcher, J.-F., De Maagt, P. and Gerlach, L. (2001): Combination of Antennas and Solar Cells for Satellite Communications. Microwave and Optical Technology Letters, Vol. 29, No. 1, pp. 11–16. doi: 10.1002/mop.1068.

Vaccaro, S., Mosig, J. R. and de Maagt, P. (2003): Two Advanced Solar Antenna "SOLANT" Designs for Satellite and Terrestrial Communications. IEEE Trans. on Antennas and Propagation, Vol. 51, No. 8, pp. 2028–2034. doi: 10.1109/TAP.2003.815424.

Vainio, R., Desorgher, L., Heynderickx, D., Storini, M., Flückiger, E., Horne, R. B., Kovaltsov, G. A., Kudela, K., Laurenza, M., McKenna-Lawlor, S., Rothkaehl, H. and Usoskin, I. G. (2009): Dynamics of the Earth's Particle Radiation Environment. Space Science Reviews, Vol. 147, pp. 187–231. doi: 10.1007/s11214-009-9496-7. ISSN 00386308.

Walter, C. L. (1978): Investigation of Methylpentene Polymer (tpx) Molding Resin. Available at: https://www.osti.gov/servlets/purl/5094724 (accessed Aug. 22, 2024).

Wertz, J. R., Everett, D. F. and Puschell, J. J. (2011): Space Mission Engineering: The New SMAD. "Space Technology Library," Microcosm Press. ISBN 9781881883159.

Wu, B., Sun, X.-Y., Zu, H.-R., Zhang, H.-H. and Su, T. (2022): Transparent Ultrawideband Halved Coplanar Vivaldi Antenna with Metal Mesh Film. IEEE Antennas and Wireless Propagation Letters, Vol. 21, No. 12, pp. 2532–2536. doi: 10.1109/LAWP.2022.3200455.

Xu, G., Ke, Z., Zhuang, C., Li, Y., Cai, R., Yang, Y. and Du, X. (2023): Measurements and Analysis of Solar Spectrum in Near Space. Energy Repts., Vol. 9, pp. 1764–1773. Available at: https://www.sciencedirect.com/science/article/pii/S2352484723005929 (accessed Aug. 22, 2024). doi: https://doi.org/10.1016/j.egyr.2023.04.229. ISSN 2352-4847.

Yao, J., Liu, Q., Qian, H. and Zhang, D. (2024): Dual Band Flexible Transparent Microstrip Patch Antenna Based on Metal Mesh, in Proc. 6th IEEE Int. Conf. on Communications, Information System and Computer Engineering (CISCE), pp. 126–129.

Yao, Y., Chen, W., Chen, X. and Yu, J. (2017): Design of Optically Transparent Antenna with Directional Radiation Patterns. Int. J. of Antennas and Propagation, Vol. 2017, No. 1, p. 8125432. doi: 10.1155/2017/8125432.

Yasin, T. (2013): Transparent Antennas for Solar Cell Integration. PhD thesis, Dept. of electrical and Computer Engineering, Utah State University, Logan, UT.

Yasin, T., Baktur, R., Turpin, T. and Arellano, J. (2017): Analysis and Design of Highly Transparent Meshed Patch Antenna Backed by a Solid Ground Plane. Progress In Electromagnetics Research M, Vol. 56, pp. 133–144. doi:10.2528/PIERM16092708.

Zaplotnik, R., Vesel, A. and Mozetič, M. (2018): Atomic Oxygen and Hydrogen Loss Coefficient on Functionalized Polyethylene Terephthalate, Polystyrene, and Polytetrafluoroethylene Polymers. Plasma Processes and Polymers, Vol. 15, No. 9, p. 1800021.

Zarbakhsh, S., Akbari, M., Farahani, M., Ghayekhloo, A., Denidni, T. A. and Sebak, A.-R. (2020): Optically Transparent Subarray Antenna Based on Solar Panel for Cubesat Application. IEEE Trans. on Antennas and Propagation, Vol. 68, No. 1, pp. 319–328. doi: 10.1109/TAP.2019.2938740.

Zyla, P. A. et al. (2020): Review of Particle Physics. PTEP, Vol. 2020, p. 083C01. doi: 10.1093/ptep/ptaa104.